The Global Seismic Moment Rate of Mars after Event S1222a

M. Knapmeyer[1], S. Stähler[2], A.-C. Plesa[1], S. Ceylan[2], C. Charalambous[3], J. Clinton[4], N. Dahmen[2], C. Durán[2], A. Horleston[5], T. Kawamura[6], D. Kim[2], J. Li[7], M. Plasman[6], G. Zenhäusern[2], R. C. Weber[8], D. Giardini[2], M. P. Panning[9], P. Lognonné[6], and W. B. Banerdt[9]

[1] DLR Institute for Planetary Research, Berlin, Germany. [2] Institute of Geophysics, ETH Zürich, Sonneggstrasse 5, 8092 Zürich, Switzerland. [3]Department of Electrical and Electronic Engineering, Imperial College London, South Kensington Campus, London, SW7 2AZ, United Kingdom. [4]Swiss Seismological Service (SED), ETH Zurich, Sonneggstr. 5, 8092 Zürich, Switzerland. [5]School of Earth Sciences, University of Bristol, Wills Memorial Building, Queens Road, Bristol BS8 1RJ, UK. [6]Université de Paris, Institut de physique du globe de Paris, CNRS, F-75005 Paris, France. [7]Department of Earth, Planetary, and Space Sciences, University of California, Los Angeles, California, USA. [8]NASA MSFC, NSSTC Mail Code ST13, 320 Sparkman Drive, Huntsville, AL 35805, USA [9]Jet Propulsion Laboratory, California Institute of Technology; 4800 Oak Grove Dr., M/S 183-301, Pasadena, CA 91109, USA

Corresponding author: Martin Knapmeyer (martin.knapmeyer@dlr.de)

Key Points:

- A single large marsquake suffices to constrain the global seismic moment rate
- Pre-InSight estimations tended to overestimate the moment rate
- Either a significant part of the ongoing deformation occurs silent, or seismic activity is restricted to some activity centers, or both.

Abstract

The seismic activity of a planet can be described by the corner magnitude, events larger than which are extremely unlikely, and the seismic moment rate, the long-term average of annual seismic moment release. Marsquake S1222a proves large enough to be representative of the global activity of Mars and places observational constraints on the moment rate. The magnitude-frequency distribution of relevant Marsquakes indicates a b-value of 1.17, but with its uncertainty and a volcanic region bias, $b = 1$ is still possible. The moment rate is likely between $1.5 \times 10^{15}\ Nm/a$ and $1.6 \times 10^{18}\ Nm/a$, with a marginal distribution peaking at $4.9 \times 10^{16}\ Nm/a$. Comparing this with pre-InSight estimations shows that these tended to overestimate the moment rate, and that 30 % or more of the tectonic deformation may occur silently, whereas the seismicity is probably restricted to localized centers rather than spread over the entire planet.

Plain Language Summary

The seismic moment rate is a measure for how fast quakes accumulate deformation of the planet's rigid outer layer, the lithosphere. In the past decades, several models for the deformation rate of Mars were developed either from the traces quakes leave on the surface, or from mathematical models of how quickly the planet's interior cools down and shrinks. The large marsquake that occured on the 4th of May 2022 now allows a statistical estimation of the deformation accumulated on Mars per year, and thus to confront these models with reality. It turns out that, although there is a considerable overlap, the models published prior to InSight tend to overestimate the seismic moment rate, and hence the ongoing deformation on Mars. Possible explanations are that 30 % or more of the deformation occurs silently, i.e. without causing quakes, or that not the entire planet is seismically active but only specific regions.

1 Introduction

Seismic activity is an expression of current tectonic processes on a planet. A most obvious quantification is the number of seismic events, and their characterization in terms of magnitude. One of the science objectives of the SEIS instrument aboard InSight is indeed to "Determine the rate of seismic activity" of Mars (Lognonné et al., 2019).

Seismic moment is a measure of the permanent deformation associated with a quake, and magnitude is essentially it's logarithm. Landforms of tectonic origin represent deformations accumulated in the past, and thus the cumulative seismic moment of many quakes. Comparing the current rate of accumulation with existing landforms thus connects past and present.

Up to 2020, all estimations of today's martian moment rate were based on modeling or indirect evidence: the seismic data from Viking (Anderson et al, 1977, Goins & Lazarewicz, 1979), geological evaluation of surface structures (Golombek et al., 1992, Golombek, 2002, Taylor et al., 2013), or geodynamic modeling (Phillips, 1991, Knapmeyer et al., 2006, Plesa et al., 2018). Of the latter, Knapmeyer et al. (2006) and Plesa et al. (2018) aimed at delineating the entire plausible parameter space, rather than defining a most likely result.

A first estimation based on InSight data was presented by Banerdt et al. (2020), although in terms of a magnitude-frequency distribution rather than seismic moment rate. At that time, several extrapolation steps were necessary to obtain a global annual event rate from 13 regional

events. In this work we follow a different approach that avoids extrapolation as far as possible. Our goal is to estimate the global seismic moment rate.

2 Methods and Results

The events used for the estimation of the global seismic moment rate must be representative for the global endogenous seismicity, and hence comply with two criteria: They have to be detectable at any time, and they have to be detectable (with SEIS) from any location. The first criterion applies to the Signal-to-Noise ratio (SNR) at the site of the seismometer, the second criterion involves epicentral distance and therefore applies to the magnitude of the event. In addition, impacts and other non-tectonic events have to be discarded.

We use a catalog snapshot covering the time from 02. Feb. 2019 to 06. July 2022 (1190 terrestrial days) and containing 2706 events. The first published catalog listing S1222a is the 12th catalog (InSight Marsquake Service, 2022) which covers the time up to 30.06.2022. Our snapshot has 6 additional but irrelevant SHF events (see catalog for type and quality class definitions). Two major instrument downtimes (28. Aug. 2019 to 18. Sep. 2019, and 07. Jan. 2022 to 30. Jan. 2022) and a number of data downlink interruptions reduce the effective observation time to 1128 days. Magnitudes and their uncertainties are taken as listed in the catalog.

We discard all 1696 quality "D" events which, by definition, are spurious detections that might represent wind gusts and other disturbances. We discard all 1389 events of SHF type, which are considered to represent thermal cracking within the soil in the vicinity of the lander (Dahmen et al., 2020). We further discard events identified as impacts by Garcia et al., (2022), Kim et al. (2022), and Posiolova et al. (2022), 70 VHF events the nature of which is unclear and still under investigation, and 1153 HF events. Although we consider the latter as predominantly tectonic (Stähler et al., 2022), we discard them *a priori* since they are so small that they would be discarded by magnitude and amplitude criteria anyway. Finally, 68 events from the "low frequency" (LF) family remain for further analysis, 52 with known magnitudes.

2.1 Event Selection: Detectable at any Time

We compute the noise RMS (root mean squared) ground displacement amplitude in consecutive windows of 2 min duration over the entire observation period. For convenience, we convert it into dB with respect to a reference displacement of 1 m. Due to the variability of wind speeds between seasons, and also between day and night, the RMS amplitude varies over a range of approx. 40 dB (Figure 1a, b). From the time series of RMS amplitudes, we compute the cumulative distribution function (CDF) of amplitudes (Figure 1c). This CDF is below $-185.8\ dB$ for 95 % of the time. Evaluation of the distribution of the SNR ratio suggests that we detected all events with an SNR exceeding 2, thus an allowance of about 6 dB on the noise level must be considered. A total of 8 events exceeds the resulting threshold amplitude of $-179.8\ dB$ (S0173a, S1022a, S1133c, S1157a, S1157b, S1157c, S1197a, S1222a), whereas event S0976a, with $\Delta = 146°$ and a magnitude of 4.2 ± 0.3 (Horleston et al. 2022), was removed due to its SNR.

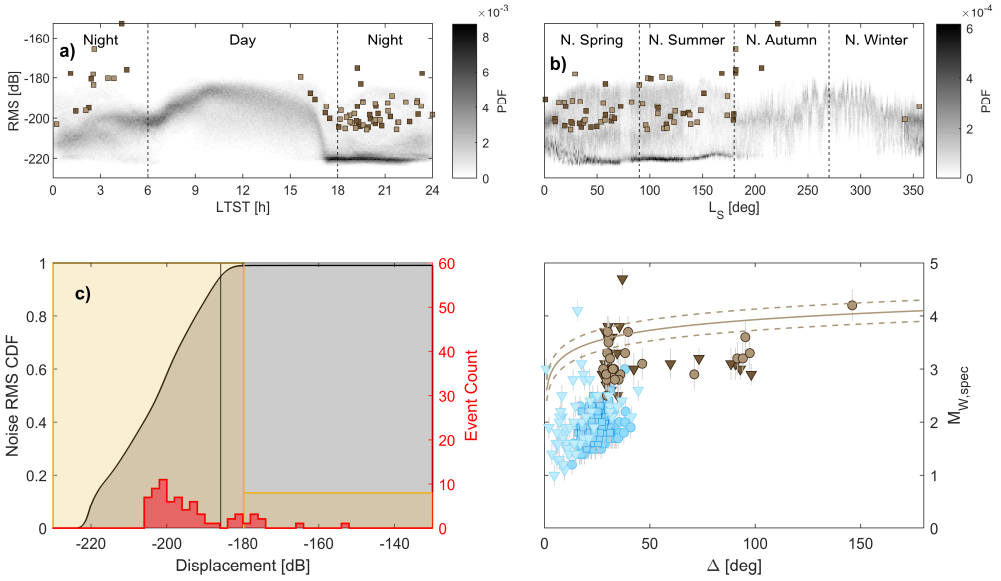

104

105 *Figure 1 Event selection criteria. a) background: histogram of displacement RMS amplitudes*
106 *throughout the sol (squares: LF (bright) and BB (dark) event amplitudes). LTST is local sun*
107 *clock time. b) background: displacement RMS amplitudes throughout the martian year, L_S is the*
108 *areocentric longitude of the Sun, symbols as in (a). c) gray: noise RMS cumulative distribution,*
109 *red: histogram of event amplitudes in 2 dB bins. 95% of all noise amplitudes are left of the black*
110 *vertical line. yellow: histogram of event amplitudes binned such that the right bin contains all*
111 *events with amplitude 6 dB (i.e. SNR 2) above 95% level. d) Event magnitudes, including their*
112 *individual uncertainties (square colors as in (a), blue triangles: VF, squares: HF events. Solid*
113 *curve: Amplitude of the weakest of the surviving events from (c) (S1197a), converted to moment*
114 *magnitudes for all distances. Dashed: as the solid curve, but factoring in the magnitude*
115 *uncertainty.*

116 2.2 Event Selection: Detectable from Anywhere

117 For two of the eight remaining events, it was not possible to estimate the epicentral
118 distance (quality "C" events). From the other six, we identify the one with the smallest recorded
119 amplitude (S1197a). We convert this amplitude into the magnitude an event needs to have at any
120 distance from 0° to 180° to be recorded with the observed amplitude, using the body wave
121 magnitude equation of Böse et al. (2021). We thus obtain a detection threshold magnitude as
122 function of distance (Figure 1d). Evaluating the equation for $\Delta = 180°$, we find that an event with
123 a magnitude of 4.1 ± 0.2 would be detectable anywhere on Mars, and, based on the events used
124 to determine the threshold, during 95% of the time. In the following we assume a threshold of
125 4.1. It is remarkable that this is more than 2 magnitudes below the Anderson et al. (1977)
126 estimation for Viking (with a short period seismometer installed on the lander platform).

127 Only one event, S1222a ($M_W = 4.7 \pm 0.2$, Kawamura et al., this special collection), is
128 above both amplitude and magnitude thresholds.

2.3 b-value and Moment Rate estimation

With only one event left, we have to resort to the NLVR (*N*ormalized *L*argest e*V*ent eve*R*) estimator of Knapmeyer et al. (2019), which assumes that the cumulative moment-frequency distribution follows a tapered Gutenberg-Richter (TGR) distribution with corner moment M_{max} and magnitude of completeness M_c, such that the relative number Φ of events exceeding magnitude M is

$$\Phi(M) = \left(\frac{M_c}{M}\right)^{\beta} exp\left(\frac{M_c - M}{M_{max}}\right) \text{ for } M_c \leq M \leq \infty \quad (1)$$

When written as function of b-value, largest observed magnitude M and number of years, n, the moment rate $\dot{M}$ is estimated as

$$\dot{M} = \frac{1}{n}\frac{\Gamma(2-2b/3)}{1-2b/3} 10^{9.1+3M/2} \quad (2)$$

The magnitudes listed in the MQS catalog are calibrated as moment magnitudes (Böse et al., 2021). The catalog gives magnitude uncertainties, in terms of the half width of a boxcar distribution, i.e. the true magnitude is within $\pm\Delta m$ magnitude units of the catalog value (not to be confused with the catalog resolution δm). This results in a lower and an upper bound for $\dot{M}$ by multiplication with $10^{\pm 3\Delta m/2}$, which, with $\Delta m = 0.2$ for S1222a, amounts to factors of 0.5 and 2 (to within a few permille), respectively.

To estimate b, we use all 52 low frequency events with known magnitudes and propagate their magnitude uncertainties: We first produce a number of perturbed magnitude lists, where a random perturbation is added to each magnitude entry to account for the magnitude roundoff and the catalogued magnitude uncertainty. For each of the perturbed catalogs, we evaluate a modified version of the well-known maximum-likelihood solution for b,

$$b = \frac{log_{10} e}{\bar{m} - (M_c - \delta m/2)} \quad (3)$$

where

$$\bar{m} = \frac{1}{N}\sum_{i=1}^{N} M_i \quad (4)$$

with magnitudes of the $N = 52$ catalogued events with magnitudes above the magnitude of completeness. Instead of estimating M_c from the catalog, we simply increment it from a value that is certainly too low to the largest value that still allows to evaluate the standard deviation of b after Shi & Bolt (1982), which is undefined for less than 3 events. We assume with Cao & Gao (2002) that the resulting b-curve will form a plateau when the assumed M_c exceeds the true value, but we don't think that the evaluation of the formal uncertainty of b is a meaningful criterion to identify the plateau with a catalog as small as ours. Instead we define a reasonable interval $2.9 \leq M_c \leq 3.3$ by visual inspection of Figure 2c, and analyze the distribution of b-values resulting from our ensemble for perturbed catalogs for M_c within that interval.

The mentioned modification of the maximum likelihood solution accounts for the fact that almost all events would be undetectable at typical daytime noise levels. Taking the catalog as-is would probably underestimate the b value, as predominantly the small events are missing

from the catalog and thus the small-events end of the magnitude-frequency distribution is biased towards low counts. We account for this by upweighting small events.

For each given event, the reciprocal of the cumulative distribution of the noise RMS amplitude, $CDF(A)$ (Figure 1c), indicates during how much of the time it would have been detectable. A simplistic way to mitigate the lack of events would be to insert a number of artificial entries to increase the number of small events and then evaluate this mended catalog. A more precise way is to replace the arithmetic mean $\bar{m}$ with a weighted mean

$$\widetilde{m} = \frac{1}{\widehat{N}} \sum_{i=1}^{N} g_i M_i \quad (5)$$

where $\widehat{N} = \sum_{i=1}^{N} g_i = 82.86$, and

$$g_i = \frac{1}{CDF(A_i)} \quad (6)$$

with the amplitude A_i of the i-th event. The weights g_i range from 1.01 to 2.04 (Figure 2a). When evaluating the formal standard deviation, $\widehat{N}$ has to be used instead of N as well. This modification corrects for the loss of events during high noise times. We do not attempt to correct for undetectably small events at large distances also missing from the catalog, since we lack the necessary information.

Each magnitude listed in the catalog carries an individual uncertainty, which, by construction, is assumed to be boxcar distributed. This further affects the estimation of b as it implies a certain fuzziness of the magnitude-frequency distribution (Figure 2b). To account for this, we evaluate not only the nominal magnitudes of the catalog, but also a large number of perturbed catalogs, where each magnitude entry is modified with a random offset drawn from a boxcar distribution with a width according to the individual event's magnitude uncertainty (Figure 2c). We do not show the formal standard deviation of b here, which grows hyperbolically towards the right of Figure 2c, when the number of events used decreases. The width of the b-value distribution in Figure 2c roughly corresponds to three formal σ.

From all b-values entering the plateau region of Figure 2c (between the dotted verticals), we finally obtain a PDF of b values (Figure 2d) which has its maximum at $b = 1.17$ (mean $\bar{b} = 1.2$, $\sigma_b = 0.135$). We emphasize that this estimation is based on events in a relatively young, possibly just dormant volcanic region of Mars (Stähler et al., 2022, and references therein). Volcanic regions on Earth often exhibit a b-value elevated with respect to the global average. Although the PDF shows only a $\approx 5\%$ probability for $b \leq 1$, we think that, given the Cerberus-Fossae-bias of the underlying data set, we cannot rule out a global average of $b = 1$, which, as global average for Earth, was assumed in pre-InSight seismicity models.

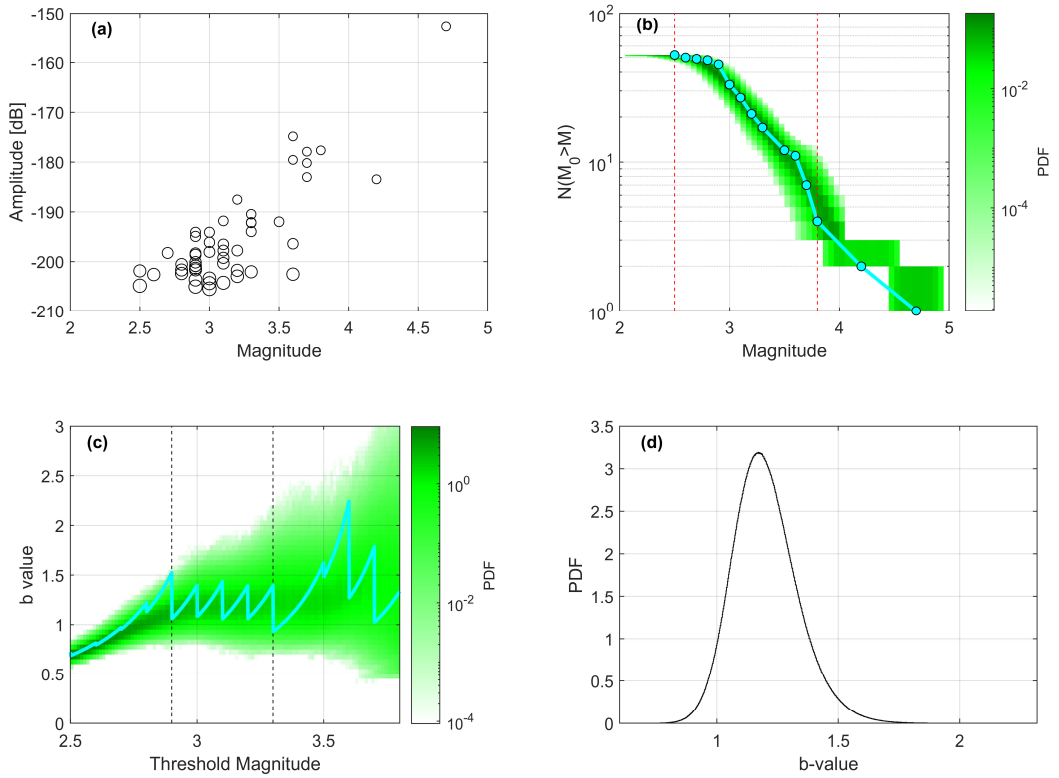

Figure 2: b-value estimation. (a) Amplitude-dependent weights of each event, symbol area is proportional to weight. (b) Cumulative distribution of Magnitudes. Line and circles: nominal values from catalog. Background: 50000 *Random perturbations of catalog magnitudes. Dashed lines: scan interval for assumed magnitude of completeness. (c) Line: b-value curve resulting from nominal catalog magnitudes. The sawtooth shape results from stepwise reduction of included events. Background: PDF of curves resulting from perturbations of the catalog. Vertical dotted lines: Plateau zone of near constant b. (d) Distribution of b-values from within the plateau zone of panel (c).*

We now have all parameters for the evaluation of eq. 2 at hand. Inserting $n = 1128/365.25$, $M = 4.7$, and $b = 1.17$, we obtain $\dot{M} = 1.9 \times 10^{16}\ Nm/a$ (where a refers to terrestrial years), and the magnitude uncertainty $\Delta m = 0.2$ results in upper and lower bounds

$$9.5 \times 10^{15}\ Nm/a \leq \dot{M} \leq 3.8 \times 10^{16}\ Nm/a \quad (7)$$

With $b = 1.0$ we obtain $\dot{M} = 1.2 \times 10^{16}\ Nm/a$ and bounds

$$6.1 \times 10^{15}\ Nm/a \leq \dot{M} \leq 2.4 \times 10^{16}\ Nm/a \quad (8)$$

The catalog is only one realization of a random process drawing from the moment-frequency distribution, which also depends on the corner moment. We need to estimate how the probability to obtain the observed moment rate after ≈ 3 years depends on the choice of *both* parameters of the TGR distribution, and how the parameters trade off against each other.

To this end, we scan the parameter space defined by $\dot{M}$ and M_{max} on a regular grid, where both parameters are expressed as equivalent magnitudes according to $M_w = (log_{10}M_0 - 9.1) * 2/3$. For a given b-value, each node of this grid defines a TGR. We generate 2000 synthetic event TGR catalogs per node and evaluate eq. 2, to obtain a distribution of NLVR estimations. These estimations are compared with the above intervals to obtain the desired probabilities, called emission probabilities by Knapmeyer et al. (2019). Figure 3 shows these probabilities in the moment-rate-corner-magnitude parameter space and in the form of the corresponding cumulative size-frequency distributions for both $b = 1.17$ and $b = 1.0$.

Most parameter combinations are very unlikely to produce the NLVR moment rate intervals of eqs. 7 and 8 (white in Figure 3a and c), this includes the "Medium", "StrongFew" and "StrongMany" models of Knapmeyer et al. (2006).

Feasible parameter combinations are found in an *L*-shaped region, with a short horizontal arm (in Figure 3a and c) where the emission probability actually reaches 1, and a near vertical arm along which the emission probability hardly exceeds 40%, but which extends towards high corner moments indefinitely. We set an arbitrary cutoff for our grid search at $M_{max} = 8$, but it is easy to extrapolate to higher values at will. Towards low corner moments, we set a cutoff at the lower bound of the magnitude uncertainty of S1222a, i.e. at $M_{max} = 4.5$. An even lower value of M_{max} would imply that we already saw the largest event possible on Mars - it is safe to assume that we didn't.

The highest emission probabilities are found for corner moments below the mean magnitude of S1222a and moment rates slightly above having one event like S1222a per year.

The marginal distributions at the bottoms of Figure 3a and c indicate the moment rates which most likely reproduce the observed NLVR range. When requiring a minimum emission probability of 0.1, the moment rate is bounded upwards by an equivalent magnitude of 6.25 ($b = 1.17$, $2.5 \times 10^{18}\ Nm/a$), whereas a moment rate equivalent of 5.06 ($4.9 \times 10^{16}\ Nm/a$) is most likely to reproduce the observation. The marginal distribution does not rule out a moment rate below that of the Shallow Moonquakes (3.8), although this is very unlikely. Emission probabilities above 10% are found only for moment rates between equivalent magnitudes of 4.1 ($1.7 \times 10^{15}\ Nm/a$) and 6 ($1.26 \times 10^{18}\ Nm/a$). A higher upper bound would imply to consider possible Marsquakes with magnitudes above 8. Even Cerberus Fossae, which appears to be the seismcially most active region at least on the InSight hemisphere of Mars, does currently not make us expect events of this size (see also Stähler et al., 2022), although the longest grabens on Mars are long enough to accommodate magnitude 9 events (according to the Knapmeyer et al., 2006, fault catalog).

The increasing dust load on InSight's solar arrays made continuous operation of SEIS increasingly difficult in 2022. A 10 sols data gap begins two sols after S1222a: Under slightly different weather conditions we might have missed this event altogether. We repeat our analysis under the assumption that S0976a, although marginally below our acceptance thresholds, is still the largest observed event by July 2022. As expectable with the larger magnitude uncertainty of S0976a, we obtain a wider rate range with emission probabilities above 10% (3.4 to 6.5 in terms of magnitude). The smaller magnitude of S976a makes the marginal distribution peak at a smaller rate (4.6).

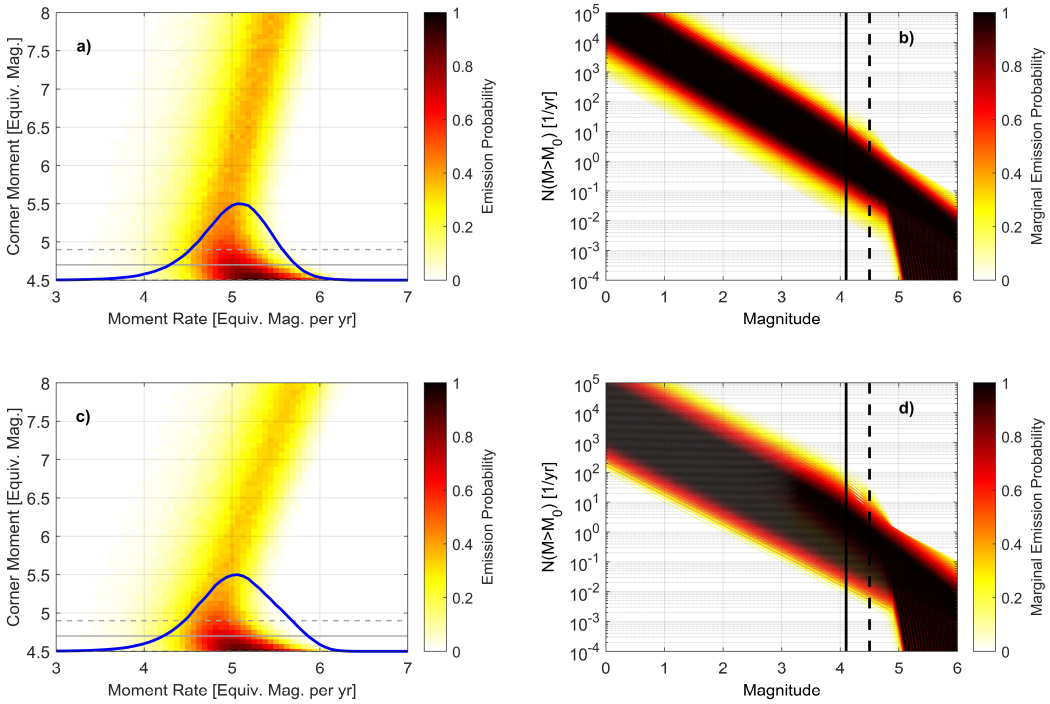

Figure 3: Feasible combinations of moment rate and corner moment, converted to magnitudes. (a) Emission probabilities for $b = 1.17$. Emission probabilities as function of moment rate and corner moment, estimated from 2000 synthetic catalogs per pixel. Horizontal lines indicate the magnitude of S1222a and its uncertainty. At the bottom: marginal emission probability as function of moment rate. (b) Parameter space depicted in the form of moment-frequency distributions, colored by marginal emission probability. Same in (c) and (d), but for $b = 1.0$.

3 Discussion

Compared to pre-InSight estimations (Figure 4), our moment rate is in the middle to lower part of their intervals, and even below those: All earlier publications tended to overestimate the moment rate. For some cases, this is easily explained by the discrepancy between geodetically observable and seismic deformation: only some fraction of all tectonic deformation causes quakes, even on Earth. The seismic moment rate only reflects brittle, but not ductile deformation, whereas a reconstruction of crustal deformation from geologic mapping also includes the latter.

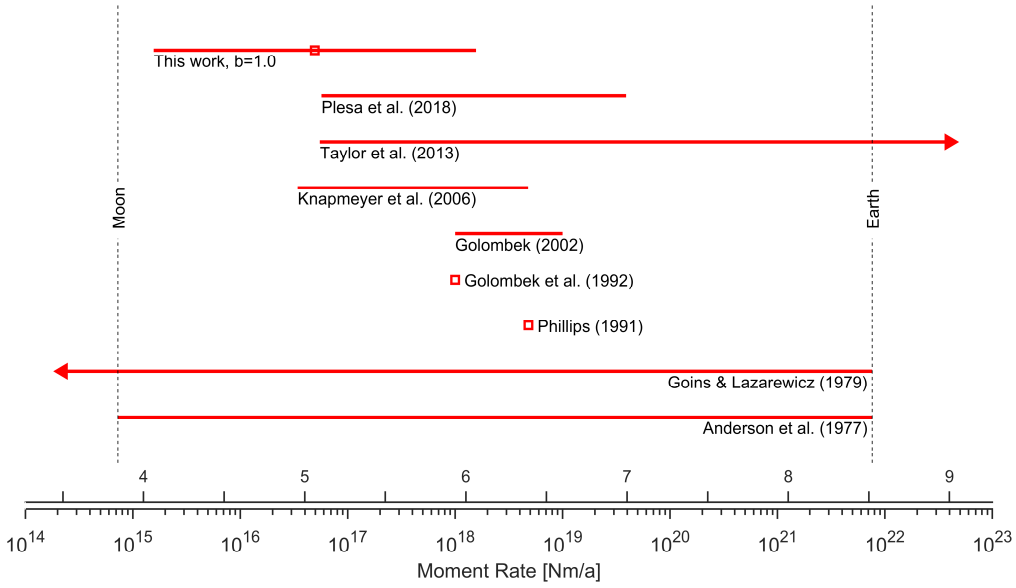

Figure 4: Comparison of published moment rate estimations. Earlier estimations either give intervals (horizontal bars, with an arrowhead if no bound in one direction was given) or single values (squares). Our result is depicted as the interval for which the emission probability in the $b = 1.0$ *case exceeds 10%, and the maximum of the marginal distribution is indicated by a square. Values from Earth and Moon from Knapmeyer et al. (2019). Rulers give the moment rate in Nm/a and as equivalent moment magnitude.*

This applies to the estimations of Golombek et al. (1992), Golombek (2002), and Taylor et al. (2013). The latter estimated the moment rate of the Cerberus Fossae formation only but did not define an upper bound for the planetary moment rate.

The Viking non-observation of seismicity did not allow to derive tight constraints. The resulting estimations (Anderson et al., 1977, and further detailed by Goins and Lazerewicz, 1979) were both focused on event rate rather than moment rate.

One might of course argue that the Earth's moment rate (and the derived event rate) must be larger than that of Moon and Mars just because of the planet's sizes.

The appropriate framework for a size-dependent moment rate scaling is the equation of Kostrov (1974, see also Bratt et al., 1985), which also underlies the predictions for Mars from thermal evolution models. According to this equation, the moment rate is proportional to strain rate and seismogenic volume - which is not easy to determine. In terrestrial oceanic crust, the seismic nucleation depth appears to be limited by the 600°C isotherm (Abercrombie & Ekström, 2001, McKenzie et al., 2005), so one could estimate the seismogenic volume of oceanic crust from thermal models thereof for the entire surface covered by it. Kreemer et al. (2000) however show that a much smaller volume derived from the world strain map suffices to explain the Earth's seismic moment rate from observed strain rates.

Our knowledge of nucleation depths on the Moon appears patchy, at best, when comparing the source depths of shallow moonquakes found by different authors (e.g. Knapmeyer & Weber, 2015, and references therein). Little do we know about Mars, but enough to conclude

that when taking the entire lithosphere above the 600°C isotherm, the resulting volume would exceed the Kreemer et al. volume for the Earth, whereas taking the source depth estimations of Brinkman et al (2021) and Jacob et al. (2022), which are 40 km or less, as upper limit, the resulting volume would be smaller than what we get for the Moon with a seismogenic depth of 300 km. We therefore think that our knowledge is insufficient to derive a proper scaling relation between the Moon, Mars, and the Earth. Taken in absolute terms, the moment rates of Moon and Earth turn out as valid brackets for the martian one, nevertheless.

Phillips (1991), Knapmeyer et al. (2006), and Plesa et al. (2018) based their estimations on increasingly complex thermal evolution models. Knapmeyer et al. introduced a seismic efficiency factor η to decouple brittle and ductile deformation, but only crude estimations of this factor could be made, which did not change with Plesa et al. Both did not expect the low moment rates we must consider possible after three years of InSight observations.

Without additional constraints, a low rate can still be attributed to a low seismic efficiency. In the model of Knapmeyer et al. (2006), as long as the seismogenic lithosphere is thin (less than about 300 km) the moment rate $\dot{M}$ is proportional to shear modulus ($\mu = 30 \ldots 70\ GPa$), cooling rate ($\dot{T} = (0.2 \ldots 1.1) \times 10^{-7}\ K/a$), thermal expansion coefficient ($\alpha = (2 \ldots 3) \times 10^{-5}\ 1/K$), seismogenic lithosphere thickness ($h = 40 \ldots 150\ km$), and $\eta = 0 \ldots 1$, i.e. $\dot{M} \propto \eta\mu\alpha h\dot{T}$. Within the above parameter ranges of Knapmeyer et al. (2006), the only way to have a moment rate of $4.9 \times 10^{16}\ Nm/a$ or less is indeed if $\eta \leq 0.7$, or if the seismogenic volume is limited to a few active centers rather than comprising the entire planet - which is also plausible in the light of InSight's observations. Accordingly, the "StrongFew", "StrongMany", and "Medium" models of Knapmeyer et al. are all excluded by having emission probabilities below 3×10^{-4}.

Knapmeyer et al. (2006) considered their model parameters as independent of each other, which is not necessarily true. How to reconcile our moment rate with more complex thermal evolution models with realistic dependencies between parameters, will be investigated in the future.

4 Conclusions

In our estimation of the seismic moment rate of Mars, we avoided extrapolations from low noise to high noise times, and from regional to global seismicity by downselecting the recorded events to those detectable at any time and from anywhere. Unfortunately, only one event remained. Different approaches that make use of more of the detected events are possible, but will need extra assumptions and thus add extra tradeoffs. The single event nevertheless allowed deriving a feasible range of rates, which led us to the conclusion that pre-InSight publications, geologically or theoretically motivated, tended to overestimate the moment rate. Our preferred explanation for this is that either aseismic deformation occurs, or the global seismogenic volume is restricted to some centers of activity (like Cerberus Fossae) and much smaller than previously assumed, or some combination of both as known from Earth. In the future, a seismic network on Mars, but also a precise geodetic monitoring of fixed points on the surface, may help to disentangle the two effects and further clarify the tectonic processes occurring not in a distant past but today.

Acknowledgments

We acknowledge NASA, CNES, partner agencies and Institutions (UKSA, SSO, DLR, JPL, IPGP-CNRS, ETHZ, IC, MPS-MPG) and the operators of JPL, SISMOC, MSDS, IRIS-DMC and PDS for providing SEED SEIS data.

N.D., C.D., and G.Z. would like to acknowledge support from ETH through the ETH+ funding scheme (ETH+02 19-1: “Planet Mars”).

M.P.P. and W.B.B were supported by the NASA InSight mission and funds from the Jet Propulsion Laboratory, California Institute of Technology, under a contract with the National Aeronautics and Space Administration (80NM0018D0004).

A.H. is funded by the UKSA under grant numbers ST/R002096/1 and ST/W002523/1.

A.-C.P. gratefully acknowledges the financial support and endorsement from the DLR Management Board Young Research Group Leader Program and the Executive Board Member for Space Research and Technology.

This is InSight Contribution ICN 273.

Open Research

The InSight seismic event catalog version 12 (InSight Marsquake Service, 2022), the waveform data and station metadata are available from the Institut de Physique du Globe de Paris (IPGP) Datacenter and Incorporated Research Institutions for Seismology Data Management Center (IRIS-DMC; http://dx .doi.org/10.18715/SEIS.INSIGHT.XB_2016), as are the previous catalog versions. Seismic waveforms are also available from the National Aeronautics and Space Administration Planetary Data System (NASA PDS, https://pds.nasa.gov/ (http://doi.org/ 10.17189/1517570).

References

Abercrombie, R. E., Ekström, G. (2001), Earthquake slip on oceanic transform faults, *Nature*, vol. 410, 74-77, https://doi.org/10.1038/35065064

Anderson, D. L., Miller, W. F., Latham, G. V., Nakamura, Y., Toksöz, M. N., Dainty, A. M., Duennebier, F. K., Lazarewicz, A. R., Kovach, R. L., Knight, T. C. D. (1977). Seismology on Mars, *Journal of Geophysical Research*, vol. 82, no. 28, 4524–4546.

Banerdt, W. B., Smrekar, S. E., Banfield, D., Giardini, D., Golombek, M., Johnson, C. L., et al. (2020, February 24). Initial results from the InSight mission on Mars. *Nature Geoscience*. https://doi.org/10.1038/s41561-020-0544-y

Böse, M., Stähler, S. C., Deichmann, N., Giardini, D., Clinton, J., Lognonné, P., Ceylan, S., van Driel, M., Charalambous, C., Dahmen, N., Horleston, A., Kaamura, T., Khan, A., Knapmeyer, M., Orhand-Mainsant, G., Scholz, J.-R., Euchner, F., Banerdt, W. B. (2021),

Magnitude scales for marsquakes calibrated from InSight data, *Bulletin of the Seismological Society of America*, vol. 111, 3003-3015, doi: 10.1785/0120210045

Bratt, S. R., Bergman, E. A., Solomon, S. C. (1985). Thermoelastic stress: ow important as a cause of earthquaes in young oceanic lithosphere? *Journal of Geophysical Research*, vol. 90, No. B12, 20149-10260

Brinkman, N., Stähler, S. C., Giardini, D., Schmelzbach, C., Khan, A., Jacob, A., Fuji, N., Perrin, C., Lognonné, P., Beucler, E., Böse, M., Ceylan, S., Charalambous, C., Clinton, J. F., van Driel, M., Euchner, F., Horleston, A., Kawamura, T., Knapmeyer-Endrun, B., Mainsant, G., Panning, M. P., Pike, W. T., Scholz, J.-R., Robertsson, J. O. A., Banerdt, W. B. (2021), First focal mechanisms of marsquakes, *Journal of Geophysical Research Planets*, vol. 126, https://doi.org/10.1029/2020JE006546

Cao, A., Gao, S. S. (2002), Temporal variation of seismic b-values beneath northeastern Japan island arc, *Geophysical Research Letters*, vol. 29, No. 9, 1334, doi: 10.1029/2001GL013775

Dahmen, N. L., Clinton, J. F., Ceylan, S., van Driel, M., Giardini, D., Khan, A., et al. (2020). Super high frequency events: A new class of events recorded by the InSight seismometers on Mars. *Journal of Geophysical Research: Planets*, 125, e2020JE006599. https:// doi.org/10.1029/2020JE006599

Garcia, R. F., Daubar, I. J., Beucler, É., Posiolova, L. V., Collins, G. S., Lognonné, P., et al. (2022). Newly formed craters on Mars located using seismic and acoustic wave data from InSight. *Nature Geoscience*. Springer Science and Business Media LLC. https://doi.org/10.1038/s41561-022-01014-0

Goins, N. R., Lazarewicz, A. R. (1979). Martian seismicity, *Geophysical Research Letters*, vol. 6, no. 4, 368–370, doi: 10.1007/s11214-016-0321-9

Golombek, M. P. (2002). A revision of Mars seismicity from surface faulting, *33rd Annual Lunar Planetary Science Conference*, League City, Texas, 11–15 March 2002, Abstract 1244

Golombek, M. P., Banerdt, W. B., Tanaka, K. L., Tralli, D. M. (1992). A prediction of mars seismicity from surface faulting, *Science*, vol. 258, no. 5084, 979–981

Horleston, A. C., Clinton, J. F., Ceylan, S., Giardini, D., Charalambous, C., Irving, J. C. E., et al. (2022, April 1). The Far Side of Mars: Two Distant Marsquakes Detected by InSight. *The Seismic Record*, vol. 2., No. 2. https://doi.org/10.1785/0320220007

Jacob, A., Plasman, M., Perrin, C., Fuji, N., Lognonné, P., Xu, Z., Drilleau, M., Brinkman, N., Stähler, S., Sainton, G., Lucas, A., Giardini, D., Kawamura, T., Clinton, J., Banerdt, W. B. (2022), *Tectonophysics*, vol. 837, https://doi.org/10.1016/j.tecto.2022.229434

InSight Marsquake Service (2022), Mars Seismic Catalogue, InSight Mission, V12 2022-10-01. ETHZ, IPGP, JPL, ICL, Univ. Bristol, https://doi.org/10.12686/a18

Kawamura, T., Lognonné, P., Nishikawa, Y., Tanaka, S (2017), Evaluation of deep moonquake source parameters: Implication for fault characteristics and thermal state, *Journal of Geophysical Research Planets*, vol. 122, 1487-1504, doi:10.1002/2016JE005147

Kawamura, T., Clinton, J. F., Zenhäusern, G., Ceylan, S., Horleston, A. C., Dahmen, N. J., Duran, C., Kim, D., Plasman, M., Stähler, S. C., Euchner, F., Charalambous, C., Giardini, D., Davis, P., Sainton, G., Lognonné, P., Panning, M., Banerdt, W. B. (YEAR), S1222a - the largest Marsquake detected by InSight, submitted to *Geophysical Research Letters*, as part of AGU Special Collection "The Large Marsquake of Sol 1222"

Kim, D., Banerdt, W. B., Ceylan, S., Giardini, D., Lekić, V., Lognonné, P., et al. (2022, October 28). Surface waves and crustal structure on Mars. *Science*, vol. 378 https://doi.org/10.1126/science.abq7157

Knapmeyer, M., Oberst, J., Hauber, E., Wählisch, M., Deuchler, C., Wagner, R. (2006). Working models for spatial distribution and level of Mars' seismicity, *Journal of Geophysical Research*, vol. 111, no. E11006, doi: 10.1029/ 2006JE002708

Knapmeyer, M., Knapmeyer-Endrun, B., Plesa, A.-C., Böse, M., Kawamura, T., Clinton, J. F., Golombek, M. P., Kedar, S., Stähler, S., Stevanović, J., Perrin, C., Lognonné, P., Teanby, N. A., Weber, R. (2019), Estimation of the seismic moment rate from an incomplete sesimicity catalog, in the context of the InSight Mission to Mars, *Bulletin of the Seismological Society of America* , vol 109, No. 3, 1125-1147, doi: 10.1785/0120180258

Knapmeyer, M., Weber, R.C. (2015), Seismicity and interior structure of the Moon, in: Tong, V. C. H., Garcia, R. A (eds): *Extraterrestrial Seismology*, Cambridge University Press, Cambridge, UK, pp. 203-224

Kostrov, B. V. (1974). Seismic moment and energy of Earthquakes, and seismic flow of rock, Izv. Acad. Sci. USSR Phys. Solid Earth, Engl. Transl., 10, 13-21

Lognonné, P., Banerdt, W. B., Giardini, D., Pike, W. T., Christensen, U., Laudet, P., et al. (2019). SEIS: Insight's Seismic Experiment for Internal Structure of Mars. *Space Science Reviews*, vol. 215, https://doi.org/10.1007/s11214-018-0574-6

McKenzie, D., Jackson, J., Priestley, K. (2005), Thermal structure of oceanic and continental lithosphere, *Earth and Planetary Science Letters*, vol. 233, 337-349, doi:10.1016/j.epsl.2005.02.005

Parsons, B (1982), Causes and consequences of the relation between area and age of the ocean floor, *Journal of Geophysical Research*, vol. 87, B1, 289-302

Phillips, R. J. (1991). Expected rates of Marsquakes, in: *Scientific rationale and requirements for a global seismic network on mars*, LPI Tech Rept. 91-02 LPI/TR-91-02, Lunar and Planetary Institute, Houston, Texas, 35–38

Posiolova, L. V., Lognonné, P., Banerdt, W. B., Clinton, J., Collins, G. S., Kawamura, T., et al. (2022, October 28). Largest recent impact craters on Mars: Orbital imaging and surface seismic co-investigation. *Science*, vol 378, https://doi.org/10.1126/science.abq7704

Plesa, A.-C., Knapmeyer, M., Golombek, M. P., Breuer, D., Grott, M., Kawamura, T., Lognonné, P., Tosi, N., Weber, R. C. (2018). Present-day Mars' seismicity predicted from 3-D thermal evolution models of interior dynamics, Geophysical Research Letters, vol. 45, 2580–2589, doi: 10.1002/2017GL076124

Plesa, A.-C., Wieczorek, M., Knapmeyer, M., Rivoldini, A., Walterová, M., Breuer, D. (2022), Interior dynamics and thermal evolution of Mars - a geodynamic perspective, in:

460 Schmelzbach, C., Stähler, S. C. (eds.): Geophysical Exploration of the Solar System,
461 *Advances in Geophysics*, vol. 63, Academic Press, London etc., p. 179-230

462 Seton, M., Müller, R. D. Zahirovic, S., Williams, S., Wright, N. M., Cannon, J., Whittaker, J. M.,
463 Mathwes, K. J., McGirr, R. (2020), A global data set of present-day oceanic crustal age
464 and seafloow spreading parameters, *Geochemistry, Geophysics, Geosystems*, vol. 21,
465 e2020GC009214. https://doi.org/10.1029/2020GC009214

466 Shi, Y., Bolt, B. A. (1982), The standard error of the magnitude-frequency b value, *Bulletin of*
467 *the Seismological Society of America*, vol. 72, No. 5, 1677-1687

468 Stähler, S. C., Mittelholz, A., Perrin, C., Kawamura, T., Kim, D., Knapmeyer, M., et al. (2022,
469 October 27). Tectonics of Cerberus Fossae unveiled by marsquakes. *Nature Astronomy*.
470 https://doi.org/10.1038/s41550-022-01803-y

471 Taylor, J., Teanby, N., Wookey, J. (2013). Estimates of seismic activity in the Cerberus Fossae
472 region of Mars, *Journal of Geophysical Research*, vol. 118, 2570–2581, doi:
473 10.1002/2013JE004469

474 Ward, S. N. (1998). On the consistency of earthquake moment rates, geological fault data, and
475 space geodetic strain: The United States, *Geophysical Journal International*, vol. 134,
476 172-186

477 Watters, T. R, Weber, R. C., Collins, G. C., Howley, I. J., Schmerr, N. C., Johnson, C. L. (2019),
478 Shallow seismic activity and young thrust faults on the Moon, *Nature Geoscience*, vol.
479 12, 411-417, https://doi.org/10.1038/s41561-019-0362-2

480 Wright, T. J., Elliott, J. R., Wang, H., Ryder, I. (2013), Earthquake cycle deformation and the
481 Moho: Implications for the rheology of continental lithosphere, *Tectonophysics*, vol. 609,
482 504-523, http://dx.doi.org/10.1016/j.tecto.2013.07.029